

Damage characteristics of laser plasma shock wave on rear surface of fused silica glass

Xiong Shen(沈雄), Guo-Ying Feng(冯国英), Sheng Jing(景晟), Jing-Hua Han(韩敬华), Ya-Guo Li(李亚国), Kai Liu(刘锴)

Citation: Chin. Phys. B . 2019, 28(8): 085202. **doi:** 10.1088/1674-1056/28/8/085202
Journal homepage: http://cpb.iphy.ac.cn; http://iopscience.iop.org/cpb

What follows is a list of articles you may be interested in

Microwave absorption properties of Ag naowires/carbon black composites

Hai-Long Huang(黄海龙), Hui Xia(夏辉), Zhi-Bo Guo(郭智博), Yu Chen(陈羽), Hong-Jian Li(李宏建)
Chin. Phys. B . 2017, 26(2): 025207. **doi:** 10.1088/1674-1056/26/2/025207

Conditions for laser-induced plasma to effectively remove nano-particles on silicon surfaces

Jinghua Han(韩敬华), Li Luo(罗莉), Yubo Zhang(张玉波), Ruifeng Hu(胡锐峰), Guoying Feng(冯国英)
Chin. Phys. B . 2016, 25(9): 095204. **doi:** 10.1088/1674-1056/25/9/095204

Enhanced laser-induced plasma channels in air

Yanlei Zuo(左言磊), Xiaofeng Wei(魏晓峰), Kainan Zhou(周凯南), Xiaoming Zeng(曾小明),Jingqin Su(粟敬钦), Zhihong Jiao(焦志宏), Na Xie(谢娜), Zhaohui Wu(吴朝辉)
Chin. Phys. B . 2016, 25(3): 035203. **doi:** 10.1088/1674-1056/25/3/035203

Shadowgraph investigation of plasma shock wave evolution from Al target under 355-nm laser ablation

Liu Tian-Hang, Hao Zuo-Qiang, Gao Xun, Liu Ze-Hao, Lin Jing-Quan
Chin. Phys. B . 2014, 23(8): 085203. **doi:** 10.1088/1674-1056/23/8/085203

Mitigation of energetic ion debris from Gd plasma using dual laser pulses and the combined effect with ambient gas

Dou Yin-Ping, Sun Chang-Kai, Liu Chao-Zhi, Gao Jian, Hao Zuo-Qiang, Lin Jing-Quan
Chin. Phys. B . 2014, 23(7): 075202. **doi:** 10.1088/1674-1056/23/7/075202

Damage characteristics of laser plasma shock wave on rear surface of fused silica glass*

Xiong Shen(沈雄)[1], Guo-Ying Feng(冯国英)[1], Sheng Jing(景晟)[2], Jing-Hua Han(韩敬华)[1,†], Ya-Guo Li(李亚国)[3], and Kai Liu(刘锴)[1]

[1] College of Electronics and Information Engineering, Sichuan University, Chengdu 610064, China
[2] Sichuan Earthquake Administration, Chengdu 610041, China
[3] Fine Optical Engineering Research Center, Chengdu 610041, China

(Received 22 April 2019; revised manuscript received 9 June 2019; published online 10 July 2019)

The damage to the rear surface of fused silica under the action of high power laser is more severe than that incurred by the front surface, which hinders the improvement in the energy of the high power laser device. For optical components, the ionization breakdown by laser is a main factor causing damage, particularly with laser plasma shock waves, which can cause large-scale fracture damage in fused silica. In this study, the damage morphology is experimentally investigated, and the characteristics of the damage point are obtained. In the theoretical study, the coupling and transmission of the shock wave in glass are investigated based on the finite element method. Thus, both the magnitude and the orientation of stress are obtained. The damage mechanism of the glass can be explained based on the fracture characteristics of glass under different stresses and also on the variation of the damage zone's Raman spectrum. In addition, the influence of the glass thickness on the damage morphology is investigated. The results obtained in this study can be used as a reference in understanding the characteristics and mechanism of damage characteristics induced by laser plasma shock waves.

Keywords: rear surface of fused silica, laser-induced plasma, Raman spectroscopy, different thickness, finite element method

PACS: 52.50.Lp, 78.30.–j, 42.70.–a **DOI:** 10.1088/1674-1056/28/8/085202

1. Introduction

With the widespread application of high-power laser technology in industrial processing, laser weapons, and NIF systems, the laser-induced damage to optical components has received extensive attention.[1–3] In the high-power laser terminal assembly, fused silica is mainly used for making ultraviolet optical elements, such as shielding sheet (window glass), beam sampling grating (BSG), and focusing lens.[4]

Once the fused silica is damaged, the damage will rapidly increase.[5–7] Because the damage to the rear surface is more severe, the damage growth will generally appear first on the rear surface.[8] This not only limits the overall performance of a high-power laser device but also hinders the continuous increase of the output energy of high-power laser device.[9,10] The damage characteristics of fused silica have been investigated. Through the study of the damage process and dynamic behaviors, it has been found that a shock wave appears in the damage process.[11–13] This shock wave's peak pressure on the rear surface of the material is greater than that exerted on the front surface, which causes the rear surface to incur larger damage.[14] Thus, a large quantity of materials is ejected and potholes are formed. Simultaneously, radial cracks and axial crack propagation occur.[15–18] However, previous studies have mainly focused on analyzing the macroscopic damage of fused silica, and the cause of crack propagation has only rarely been analyzed in detail.[19] To date, the effect of the material thickness on the damage of the fused silica under a plasma shock wave has not yet been reported.

In this study, the effects of the material thickness on laser damage are experimentally analyzed through the different types of damage incurred by the rear surface of the fused silica with different thickness values. At the same time, the rear surface is analyzed by observing the cross-sectional damage morphology of quartz glass. Additionally, we analyze the different damage mechanisms of the fused silica, which are induced by a plasma shock wave under the action of compressive stress and tensile stress. We use a finite element software to simulate the propagation of the plasma shock wave in the fused silica, and the quartz is fractured by the plasma shock wave. The experimental results are verified by conducting numerical simulations.

2. Experiment

A schematic representation of the experimental set-up that was used to investigate the laser induced damage can be found in Ref. [20]. A He–Ne laser was used for the collimation optical path. Additionally, an Nd:YAG laser (SGR-10, LABest Optronics Co. Ltd) was used for irradiating the sam-

*Project supported by the Key Research and Development Projects of Science and Technology Department of Sichuan Province, China (Grant No. 2018FZ0032) and the National Natural Science Foundation of China (Grant No. U1730141).

†Corresponding author. E-mail: hanjinghua@scu.edu.cn

© 2019 Chinese Physical Society and IOP Publishing Ltd

ples, and the output beam profile was Gaussian with a wavelength of 1064 nm, pulse duration of 13.6 ns, spot radius of approximately 3.8 mm, and the energy fluctuations of pulsed laser below 3%. In the experiment, the Gaussian beam was focused by a quartz lens (focal length = 200 mm) and the focal spot radius was approximately 0.3 mm. The entire apparatus was completely automatic; that is, the computer could control the sample displacement, laser shot synchronization, repetition rate, and number of laser pulses. To avoid the effect of air breakdown in the experiment, we focused the laser inside the quartz optical element as close as possible to the rear surface of the quartz glass. The used energy meter was Ophir PE25. The experimental samples were two-side polished fused silica with a size of 60 mm ×30 mm and thickness ranging from 0.8 mm to 5 mm. The laser had energy of 46.8 mJ for the pulsed irradiation times of 1, 3, 5, 10, 15, and 20, separately. The damage to the quartz glass was observed by using an optical microscope (OM, Keyence, VHX650).

When the laser focused on the rear surfaces of the quartz glasses with different thickness, the morphology of the damaged area changed with the number of irradiation pulses increasing. In the experiment, we controlled the laser parameters such that the laser acting on the rear surface of the sample had the laser pulse energy of 46.8 mJ. Using a microscope, we obtained the morphology variation of the damaged surface of the fused silica rear surface with thickness. The diameter of the damage point was obtained by the measurement. Figure 1 shows comparisons of the surface topographies obtained under the same energy and number of pulses (20 pulses) for glasses with different thickness. Figure 2 shows the damage topographies of the rear surface of the fused silica with a thickness of 1 mm and different numbers of pulses.

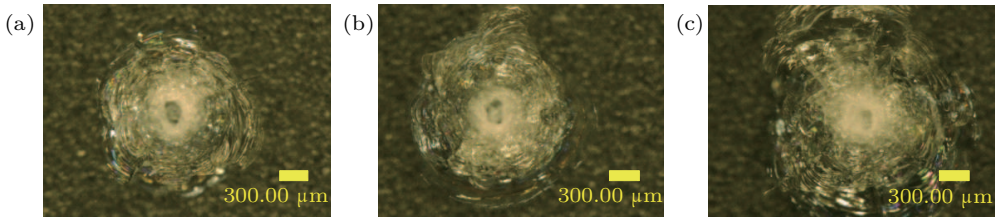


Fig. 1. Rear surface topographies of glasses with thickness of (a) 0.8 mm. (b) 1 mm, and (c) 1.4 mm under the same energy and number of pulses (20 pulses).

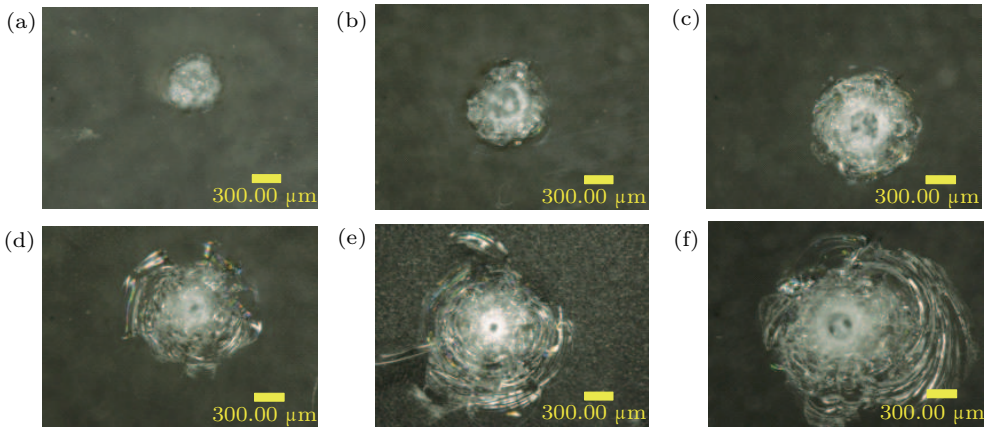


Fig. 2. Damage morphologies of 1-mm-thick fused silica surface under different numbers of pulses: (a) 1 pulse; (b) 3 pulses; (c) 5 pulse; (d) 10 pulses; (e) 15 pulses; (f) 20 pulses.

Several cases can be seen in the above experimental comparison. On all samples produced is the crater-shaped damage, and a large quantity of materials are ejected from the central region of the damage, which leads to the formation of a large pothole. Additionally, a secondary fracture occurs under the action of the laser plasma shock wave. The rear surface damage consists of a large quantity of materials sprayed onto the rear surface, and a pit is formed in the center of the damage. Moreover, obvious differences are not observed in the rear surface damage morphology of the fused silica as the thickness changes. However, the damage point sizes are different as shown in Fig. 3.

As can be seen in Fig. 3(a), the size of the damage point of the fused silica increases with the number of pulses. The damage size first increases exponentially with the number of pulses, and then the growth slows down when the number of pulses exceeds a certain number. As can be seen in Fig. 3(b), for the rear surface, the damage point size of the material increases as the thickness of the material increases. When the thickness is greater than or equal to 1.4 mm, the damage size of the material hardly changes.

As the number of pulses increases, the cross-sectional damage areas of the materials with different thickness gradually increase, and structures with different damage character-

istics are formed. Figure 4 shows the damage morphologies of the cross-section of fused silica with a thickness of 0.8 mm and different numbers of pulses.

There is no significant difference among the cross-sectional damage morphologies of fused silica with different thickness. According to the difference in topography, the cross-sectional damage zones of quartz can be divided into zones A, B, and C.[21] The cracks in the central fracture area has a large degree of intersection and many atomized small secondary cracks are formed, which is termed the atomization area (zone A). Along the outside of the atomized secondary cracks, the crack expanded outward from a line shape into a feather area (zone B). At the outer edge of the feather break zone, which is named the mirror zone (zone C), the crack suddenly disappears, and obvious fracture does not occur.

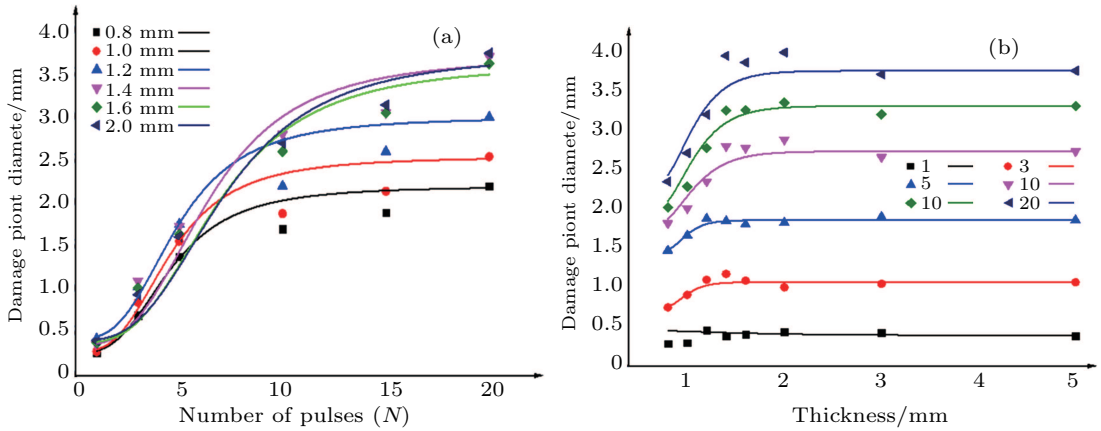


Fig. 3. Plots of variation of damage point diameter (a) with pulse number for different thicknesses (b) with thickness for different pulse times.

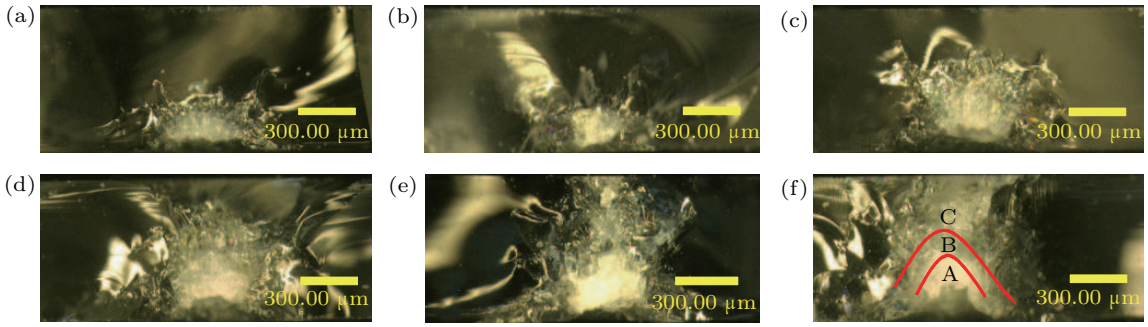


Fig. 4. Cross-section damage morphologies of fused silica (0.8 mm) under irradiation of (a) 1 pulse, (b) 3 pulses, (c) 5 pulses, (d) 10 pulses, (e) 15 pulses, and (f) 20 pulses.

3. Theoretical analysis

3.1. Characteristics of laser plasma

Fused silica belongs to a brittle solid, and its elastic pressure is on the order of thousands of atmospheres, while the pressure of laser plasma shock wave can reach several orders of a million atmosphere pressure, which is much higher than the elastic pressure.[22] There are a large number of defects or cracks inside fused silica glass. Under the high pressure of shock wave, the cracks will grow and develop into fractures rapidly.[23] At a pressure higher than 10 GPa, phase transformation and melting will happen.[24] At the same time, the change in refractive index, caused by plastic deformation, can be found in the crack tip and in the phase transition of the structure.[20] At the rear surface, the rest pulse laser light is reflected when it propagates through the plasma, and a standing wave forms on the surface of the medium, so that the ratio of light pressure to the position increases. This results in a greater pressure ratio difference between the front surface and rear surface of the optical element. Moreover, owing to the reflection of the plasma, more energy is deposited inside the material near the rear surface, which leads to more severe damage. The difference from the damage mechanism of the front surface lies in the fact that the plasma shock wave in the air is strong on the front surface, while the shielding effect of the plasma suppresses the deposition of the remaining pulse energy and reduces the damage degree of the element. The rear surface damage pit has a certain depth and a large number of cracks. Thus, compared with the front surface, the laser energy at the rear surface is easy to absorb and couple to form a stronger plasma. The residual pulse interacts with the plasma in the channel, and the resulting shock wave is confined within the damaged channel and has a greater impact pressure on the damage pit. Additionally, because the mechanical strength of the damaged material is greatly reduced, the peeling off of the material is more severe. Although the plasma generated by

the leading and trailing surface pulse front can also absorb the laser energy, their difference is that the plasma absorbing the laser energy at the rear surface encounters the glass interface when it expands. Therefore, the impact force is stronger than that at the front surface. The ratio of the pressure on the front surface to that on the rear surface, which is caused by the shock wave, is expressed as[25]

$$\frac{p_{\mathrm{f}}}{p_{\mathrm{b}}} = \left(\frac{\gamma+1}{2\gamma}\right)^{[2\gamma/(\gamma-1)]}, \tag{1}$$

where γ is the specific heat ratio when the laser plasma shock wave propagates in air, p_{f} and p_{b} are the pressure of the plasma shock wave on the front surface and that on the rear surfaces, respectively. Using this formula, it can be seen that the front-rear surface pressure ratio is approximately 1:3. The expression of the plasma shock wave pressure on the front surface is expressed as[26]

$$P = BI^{0.7}\lambda^{-0.3}\tau^{-0.15}, \tag{2}$$

where P (in unit kbar) denotes the pressure (1 bar = 0.1 MPa), I (in units GW/cm^2) the incident light intensity, λ the incident wavelength (in unit μm), τ the pulse width (in unit ns), B a constant, and $B = 21$ in the glass. The peak pressure of the plasma shock wave is 4.5 GPa. Therefore, the rear surface plasma shock wave pressure peaks approximately at 13.5 GPa.

3.2. Transmission of shock waves inside glass

The propagation of the laser induced plasma shock wave in fused silica is a complicated process. Hence, simplification is required to analyze the propagation and force distribution characteristics of the shock wave on the surface and inside the glass, and the damage morphology characteristics of the glass under different forces. Accordingly, we simplify the process of loading the shock wave into the material as an impact pressure history curve and consider it as a known condition when loading the model. The shock pressure history curve is approximately a Gaussian curve. The action time of the shock wave is approximately equal to three times the laser pulse width, which is 37.2 ns, and the shock wave peak pressure is 13.5 GPa.

The mechanical properties of the fused silica glass used in the model are listed in Table 1. A cube with a size of 5 mm ×5 mm and thickness ranging from 0.8 mm to 5 mm is created as a 1/2 model (The fused silica is cut into two symmetrical pieces along the section where the loading center is located, and one of them is selected as a model) under the assumption of symmetric boundary conditions. The other side boundary conditions are set to be no reflection. The front and rear surface are set to be free end faces. By simulating the transmission of the laser plasma shock wave inside the fused silica, the cloud profile of the time-dependent stress distribution in the material is obtained, and the characteristics of the laser plasma shock wave in the material are analyzed. The propagation process of the simulated plasma shock wave in the material is shown in Fig. 5. The propagation process undergoes the loading and propagation phase of the shock wave. When the shock wave reaches the front surface of the material, it is reflected. Because the glass and air impedance are different by several orders of magnitude, the reflection is regarded as free end reflection. The reflected wave and incident stress wave are superimposed, which causes the internal stress of the material to change and thus affect the crack propagation.

Table 1. Mechanical properties of fused silica.

Property	Value
Density/kg·m^{-3}	2200
Poisson's ratio	0.17
Elastic modulus/GPa	72.1
Tensile strength/MPa	50
Compressive strength/MPa	80–1000

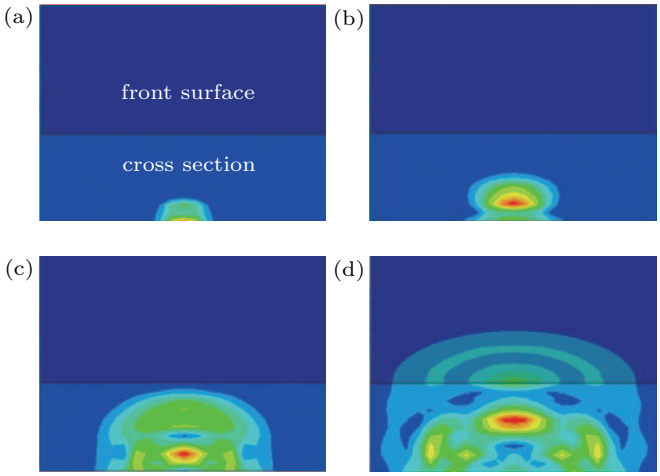


Fig. 5. Simulated plasma shock wave propagation in material, showing the scenarios of (a) load, (b) spread, (c) diffusion, and (d) reflection and overlay.

As shown in Fig. 6, for the fused silica with different thickness, the damage is also different due to the different transmission processes of the plasma shock wave. For a thicker fused silica sample, the shock wave gradually dissipates during the propagation inside and the damage processes are approximately the same. For a thinner fused silica sample, the shock wave travels directly to the rear surface and reflected shock wave will be superposed with the incident wave.[27] The impedance of the air is several orders of magnitude lower than that of fused silica, which can cause most of the energy of shock wave to reflect back.[28] The superposition of the incident with reflection wave can change the stress distribution of glass as well as the rule in forming the cracks.

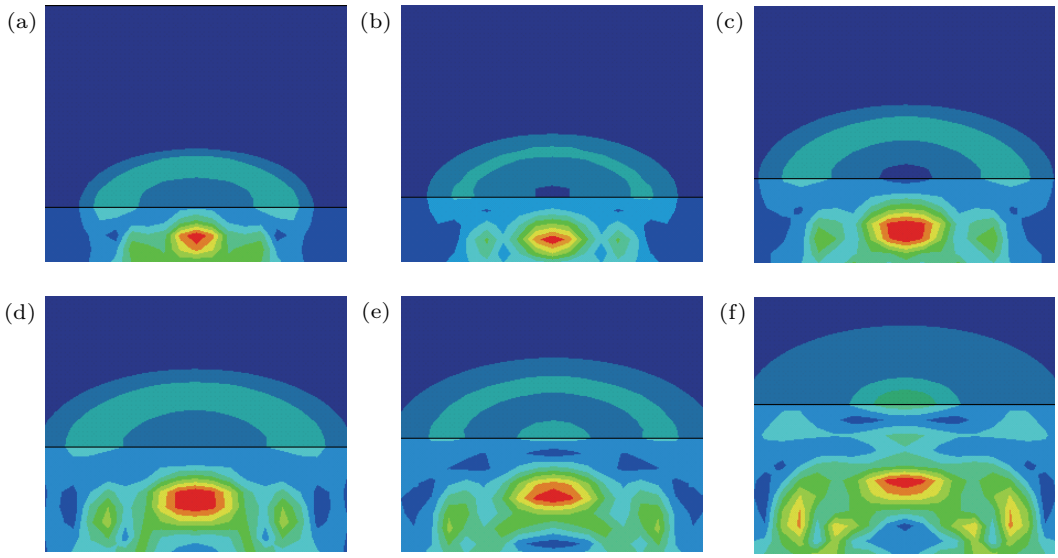


Fig. 6. Comparisons among shock waves propagating in fused silica with thickness of (a) 0.8 mm, (b) 1.0 mm, (c) 1.2 mm, (d) 1.4 mm, (e) 1.6 mm, and (f) 2.0 mm.

3.3. Damage mechanism of shock wave to fused silica glass

We analyze the cross-section damage morphology of the fused silica under a shock wave of laser plasma by simulating the stress distribution. The results are shown in Fig. 7.

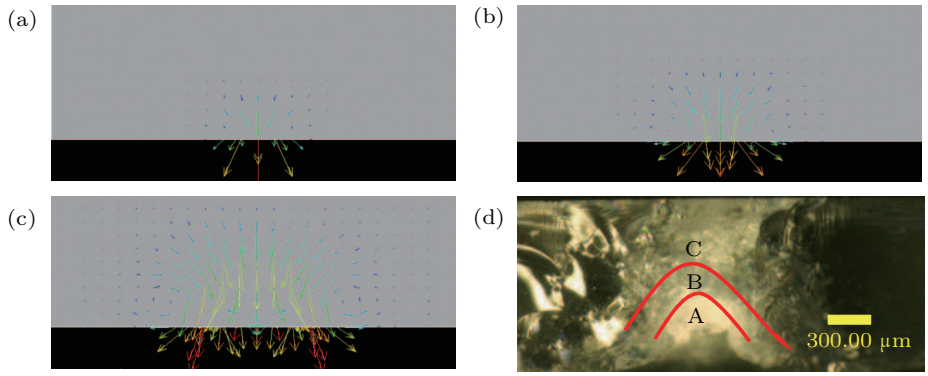


Fig. 7. Distributions of cross-sectional deformation of fused silica with 1-mm thickness at times of (a) 30 ns, (b) 60 ns, (c) 90 ns. (d) Three areas of cross-sectional damage.

The cross-section damage morphology of fused silica is observed experimentally. As can be seen in Fig. 7(d), there exist a dense layer at the bottom of the damage pit, and radial and axial cracks appearing in the material, which indicates that high-pressure shock waves appear in the material. According to the damage morphology, the damage shown in Fig. 7(d) can be divided into three zones, namely, A, B, and C. Figure 8 shows the Raman spectra and peak intensity comparison among the A, B, and C regions. By comparing the Raman spectra of the mirror area, feather area, and atomization area, it is found that the characteristic peak distributions of the Raman spectra are essentially the same. This indicates that the basic structure of the fused silica does not change significantly. However, the entire spectrum of the fault region appears as red-shift because the Si–O bond in the damaged region is broken, the x in SiO_x decreases, and the number of topological rings decreases after the broken bonds have been recombined, and the quartz optical elements are macroscopically exhibited. The densification of the overall structure leads the phase change to occur possibly. Figures 7(a)–7(c) show the deformations of the material at different times during the shock wave simulation. Figures 6(a)–6(c) represent the results at times of 30 ns, 60 ns, and 90 ns. The direction of the arrow indicates the direction of the deformation, and the length of the arrow represents the magnitude of the arrow. The closer to the center position the arrow is, the larger the represented value will be. The value can reflect the overall stress of different regions during shock wave loading. As can be seen in Fig. 7(a), the shock wave penetrates into the material and exerts a high pressure; this corresponds to area A (atomization area) in Fig. 7(d). The material undergoes a phase change and the symmetric Si–O–Si bonds of the intrinsic six-ring topology in the fused silica fracture are recombined. A smaller four- and three-ring topological structure is formed,

and the corresponding co-site and stellar quartz phases exhibit greater density. Therefore, a dense layer appears at the bottom of the damage pit. This stage is accompanied by the occurrence and expansion of axial cracks. Owing to the large stress change, the crack propagation rate is largest; therefore, the phase transformation is the most severe, and the atomization zone is formed. Figure 7(b) shows that the tensile stress occurs in the material during the shock wave propagation. Because the tensile strength of the material is smaller than the compressive strength, the material undergoes the radial crack propagation under the action of the tensile force as shown in Fig. 7(d) (zone C). At this point, the Si–O bond recombination of the material presents more quartz phases in the tricyclic topology. Owing to the small change of stress, the cracks tend to expand linearly and form a feather zone. As can be seen in Fig. 7(c), the shock wave continues to propagate. The axial cracks and radial cracks continue to expand under the influence of pressure and tensile force, and ultimately determine the damage size and damage depth of material as shown in Fig. 7(d) (zone B), where the Si–O bond fracture is relatively low. The crack growth rate drastically decreases. Additionally, the phase transition is insignificant; thus, a mirror region is formed. The topological ring structure is closely related to the phase of SiO_2. The average Si–O–Si angle will decrease after the network topology structure of fused glass has been broken and reformed. Comparing the Raman shifts of three zones, we find that the extent of red shifts of zones A, B, C increase in turn, which means that the degree of structural change of zone A is more than that of zone B. This kind of change may lead to the phase transition. Comparing with zone C, it can be found that a broad band at 478 cm^{-1} in zone B is induced by plasma shock wave, which means that the range of Si–O–Si angle as well as the fracture probability of Si–O–Si band is increased. Comparing the intensity of 607 cm^{-1} with that of 603 cm^{-1}, both of shifts represent three-number rings. and the fractured Si–O–Si band in zone B are richer than in zone A. Comparing zone A with zone B, the highest peak shifts means that the content of four-number rings of zone A is richer than that of six-number rings of zone B after the samples have been broken up and reformed, which is induced by plasma shock wave, indicating that Si–O–Si damage degree and density of zone C, zone B and zone A increase in turn. This kind of change may generate the phase transition. The peak intensity changes in A, B, and C regions indicate that the numbers of six-ring, four-ring, and three-ring structures in the three regions decrease in sequence.[21]

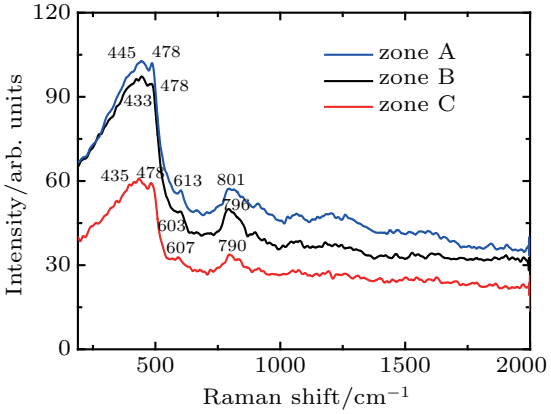


Fig. 8. Raman spectra of fracture region in fused silica.

4. Conclusions

By combining numerical simulations with experimental results, we compare the stress conditions at different times in a material with damage morphology, and we obtain the damage morphology of the rear surface of fused silica subjected to laser plasma shock waves. The damage of the rear surface is attributed to the formation of the plasma shock wave and the manner in which this wave propagates in the fused silica. The microfracture characteristics of the three regions subjected to stress are analyzed using Raman spectra, and the damage morphology of the cross-section is verified. The thickness of the fused silica affects the damage to the fused silica. As the thickness decreases, the damage to the rear surface also increases. When the thickness of the fused silica is equal to or greater than 1.4 mm, the damage to the rear surfaces is approximately the same. These results can be used as a reference for the investigation of laser induced material damage characteristics and material parameter selection in designing laser systems.

References

[1] Liao Z M, Nostrand M, Carr W, Bude J and Suratwala T I 2016 *Pacific Rim Laser Damage* 2016*: Optical Materials for High Power Lasers*, 22 July, 2016, Yokohama, Japan, p. 998304

[2] Jensen L O and Ristau D 2015 *Spie Optical Systems Design*, 24 September, 2015, Jena, Germany, p. 96280G

[3] Zhu J Q, Sun M Y, Liu C, Guo Y J, Yang L, Yang P Q, Zhang Y L, Wang B Y, Liu C, Li Y S, Ren Z Y, Liu D, Liu Z G, Jiao Z Y, Ren L, Zhang G W, Fan Q T, Feng T and Lin Z Q 2018 *Solid State Lasers Xxvii: Technology & Devices*, San Francisco, California, USA, p. 105110Y

[4] Shao Z F, Wang Y F, Xiang Z K and Rao C D 2016 *Research Progress of Large-aperture Fused Silica for High Power Laser*, November 2016, Suzhou, China, p. 102551D

[5] Huang W Q, Han W, Wang F, Xiang Y, Li F Q, Feng B, Jing F, Wei X F, Zheng W G and Zhang X M 2009 *Chin. Phys. Lett.* **26** 017901

[6] Elfallagh F and Inkson B J 2009 *J. Eur. Ceram. Soc.* **29** 47

[7] Yao P, Wang W, Huang C Z, Wang J, Zhu H T and Kuriyagawa T 2013 *Adv. Mater. Res.* **797** 667

[8] Carr C W, Radousky H B, Rubenchik A M, Feit M D and Demos S G 2004 *Phys. Rev. Lett.* **92** 087401

[9] Cai C, Zhu H, Huang J, Lv L, Ma P and He X 2016 *Appl. Opt.* **55** 2252

[10] Lou Z K, Han K, Song R, Yan B Z and Liu Z J 2017 *Laser Technology for Defense & Security XIII*, 1 May, 2017, California, USA, p. 101920O

[11] Kubota A, Caturla M J, Stolken J and Feit M 2001 *Opt. Express* **8** 611
[12] Negres R A, Feit M D and Demos S G 2010 *Opt. Express* **18** 10642
[13] Demos S G, Negres R A, Raman R N, Rubenchik A M and Feit M D 2009 *Laser-induced Damage in Optical Materials*, 31 December, 2009, Colorado, USA, p. 750418
[14] Wong J, Ferriera J L, Lindsey E F, Haupt D L, Hutcheon I D and Kinney J H 2006 *J. Non-Cryst. Solids* **352** 255
[15] Hu G H, Zhao Y A, Wei D and Ling Q 2012 *Chin. Phys. Lett.* **29** 037801
[16] Demange P, Negres R A, Raman R N, Colvin J D and Demos S G 2011 *Phys. Rev. B* **84** 054118
[17] Raman R N, Demos S G, Shen N, Feigenbaum E, Negres R A, Elhadj S, Rubenchik A M and Matthews M J 2016 *Opt. Express* **24** 2634
[18] Yang L, Xiang X, Miao X X, Li Z J, Li L, Yuan X D, Zhou G R, Lv H B and Zu X T 2015 *Opt. Laser Technol.* **75** 76
[19] Ming C, Jiang Y, Luo C S, Shi X Y, Ren W, Xiang X, Wang H J, He S B, Yuan X D and Lv H B 2012 *Chin. Phys. Lett.* **29** 044211
[20] Han J H, Li Y G, He C T, Zhang Q H, Niu R H, Yang L M and Feng G Y 2012 *Opt. Eng.* **51** 1809
[21] Hu R F, Han J H, Feng G Y, Wang Z P, Wei H, Zhao J P and Gu Q Q 2017 *Optik - Int. J. For Light Electron. Opt.* **140** 427
[22] Penner S S 2002 *J. Quant. Spectrosc. Radiat. Transfer* **76** 235
[23] Bourne N, Rosenberg, Mebar Y, Obara T and Field J 1994 *J. Physique IV Colloque* **4**(C8) 635
[24] Demos S, Staggs M, Minoshima K and Fujimoto J 2002 *Opt. Express* **10** 1444
[25] Liu H J, Zhou X D, Huang J, Wang F X, Jiang X D, Huang J, Wu W D and Zheng W G 2011 *Acta Phys. Sin.* **60** 065202 (in Chinese)
[26] Peyre P and Fabbro R 1995 *Opt. Quantum Electron.* **27** 1213
[27] Gabi B D 2007 *Shock Wave Reflection Phenomena*, 2nd edn. (Berlin: Springer) p. 342
[28] Wang Z P, Feng G Y, Han J H, Wang S T, Hu R F, Li G, Dai S Y, Zhou S Y 2016 *Opt. Eng.* **55** 105101